STRUCTURAL COMPARISON OF NICKEL ELECTRODES AND PRECURSOR PHASES

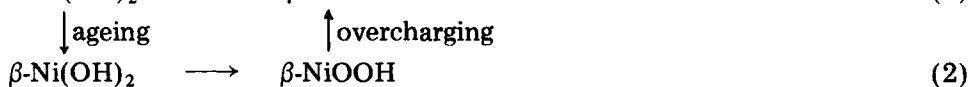BAHNE C. CORNILSEN*, XIAOYIN SHAN and PATRICIA L. LOYSELLE

Department of Chemistry and Chemical Engineering, Michigan Technological University, Houghton, MI 49931 (U.S.A.)

Summary

In this paper we summarize our previous Raman spectroscopic results and discuss important structural differences in the various phases of active mass and active mass precursors. Raman spectra provide unique signatures for these phases, and allow one to distinguish each phase, even when the compound is amorphous to X-rays (*i.e.*, does not scatter X-rays because of a lack of order and/or small particle size). The structural changes incurred during formation, charge and discharge, cobalt addition, and ageing will be discussed. The oxidation states and dopant contents are explained in terms of the nonstoichiometric structures.

Introduction

Nickel electrode active mass has traditionally been classified in terms of two distinct cycles, defined in eqns. (1) and (2) [1].

$$\alpha\text{-Ni(OH)}_2 \quad \longrightarrow \quad \gamma\text{-NiOOH} \qquad\qquad (1)$$

$$\downarrow \text{ageing} \qquad\qquad \uparrow \text{overcharging}$$

$$\beta\text{-Ni(OH)}_2 \quad \longrightarrow \quad \beta\text{-NiOOH} \qquad\qquad (2)$$

The four end-member phases have been named on the basis of X-ray diffraction pattern similarities between electrochemical materials and chemically prepared materials, α-Ni(OH)$_2$, β-Ni(OH)$_2$, and γ-NiOOH [2].

Our research has shown that these materials can be distinguished using Raman spectroscopic analysis [3, 4]. The unique spectral signatures found for the various phases allow definition of these structures and reflect significant variations. The two cycles in eqns. (1) and (2) differ in degree of nickel deficit nonstoichiometry. The nonstoichiometric structural model proposed in ref. 3 provides a framework in which the electrochemical properties can be understood. The lattice structures of active mass are non-close packed. The structural difference between the α/γ and the β/β cycles was not previously understood [5]. β-Ni(OH)$_2$, the traditional close

---

*Author to whom correspondence should be addressed.

packed model of discharged active mass, is not present in active mass. Re-analysis of the X-ray diffraction patterns for charged active mass and γ-NiOOH has supported a non-close-packed, nickel oxyhydroxide type structure, in agreement with vibrational spectra [4]. We define structural details and inter-relations between these materials, including the structures of the cobalt-containing cathodic-α and active mass [3, 6].

To distinguish the active mass structural phases from the other structures, we shall use prefixes, 2α, 3γ, 2β, and 3β [3]. This allows retention of the historical name indicative of intra-layer structure measured by the X-ray patterns, but also allows delineation of important structural differences. The structures of non-close packed active mass are defined in terms of NiO_2 layers which exhibit a nickel deficit, and therefore can contain foreign cations, and interlamellar cation sites. These are defined in terms of atom sites present in the $R\bar{3}m$, NiOOH type lattice [4]. The non-stoichiometric formulae written in this paper express these two types of sites, nickel or proton sites, and the dopants on them, by writing the former ahead of the oxygen pair and the latter after the oxygen pair.

Experimental

Preparations of the cathodic-α, ordered β-Ni(OH)$_2$, disordered β-Ni(OH)$_2$, and active mass phases (2α, 3γ, 2β, or 3β) have been described previously [3, 4]. Chemical analyses indicate that the disordered β-phases exhibit a nickel deficit ($x < 0.16$) with empirical formulae consistent with $Ni_{1-x}(2H)_x(OH)_2$. The empirical formula for cathodic-α was obtained in the same manner.

Cobalt (5%)-containing cathodic-α phase was electrochemically deposited on nickel foil (10 min) from aqueous nitrate solution (0.5 M), at a current density of 4.6 mA cm^{-2}. Cobalt-containing active mass has been produced by charging these thin films in 0.5 M KOH. The low KOH concentration minimizes ageing. Cyclic voltammetry was used to cycle the films between 0.25 and 0.55 V (with regard to a 0.5 M Hg/HgO reference electrode) at a 7.8 mV min^{-1} scan rate.

The spectra and structures for the above active mass are comparable to those found in commercial electrodes cycled to 80% depth of discharge (DOD) and charged to 120% of full charge (20% excess accounts for oxygen evolution during charge). Active mass is defined as the material, or materials, found in a "formed" electrode which is reproducibly observed during charge and discharge cycling.

Raman spectra were collected with a Ramanor HG.2S spectrophotometer with photon counting electronics. Multi-scan spectra were required to provide adequate signal-to-noise ratio. The excitation was the 514.5 nm line from an argon ion laser (10 - 20 mW on the sample).

TABLE 1

Raman band positions (cm^{-1}) characterizing solid phases present in active mass, or related to active mass [3, 4]

Spectrum type:	I	II	III	IV	V				Assignment
Structural designation:	Ordered β-Ni(OH)$_2$	Disordered β-Ni(OH)$_2$	Cathodic α-Ni(OH)$_2$	Chemical α-Ni(OH)$_2$	Active mass				
					2α	3γ	2β	3β	
	3583	3687	3650	3650					νH$_2$O
		3600							
		3580							———
		519	530		536	559	532	550	Ni–O
	453	448	462	464	470	476	468	468	lattice
	378								modes
	313	312							

Results and discussion

The band positions in the Raman spectra of active mass precursors, in active mass itself, or other related phases, are summarized in Table 1 [3, 4]. These spectra provide unique signatures allowing distinction of each phase. The basic structural unit in each of these materials is the NiO_2 layer, which contains interstitial, octahedral nickel atoms within a pair of close packed oxygen planes. For the ideal crystal lattice the proton sites are interlamellar (between NiO_2 layers); however, for a defective crystal, protons may occur within an NiO_2 layer (possibly on or near empty nickel atom sites). The structural relationship between two NiO_2 layers (layer stacking), the proton positions, and the internal structure for each NiO_2 layer influence the space group symmetry and therefore the spectral selection rules. The spectral selection rules control the number and relative intensities of the Raman and infrared vibrational bands. The 4000 - 2000 cm^{-1} region of the spectrum contains vibrational modes which reflect the symmetry and bonding of protons to oxygen atoms. The 600 - 200 cm^{-1} region of the spectrum contains Ni—O lattice modes involving motion within the two-dimensional layers. The number of lattice modes can be influenced by layer stacking interactions. The wavenumber positions of vibrational modes depend on the chemical structure and bond strengths, and therefore vary with oxidation state and/or nonstoichiometry.

Ordered and disordered β-Ni(OH)$_2$

The β-Ni(OH)$_2$ structure is the best characterized, being the only compound in this series which has been studied in single crystal form [7, 8]. The Raman spectrum (Table 1) of this highly ordered, crystalline phase contains only one O—H stretch and three lattice modes (one is very weak) [4]. This spectrum agrees with theoretical selection rules predicted on the basis of the known crystal structure. The NiO_2 layer stacking is known to be close packed in this structure. The three lattice modes originate from the intra-layer Ni—O modes and from inter-layer interaction between the close packed layers present in this stacking sequence (ABAB).

A disordered form of β-Ni(OH)$_2$ exhibits a Raman spectrum which is quite distinct in comparison with the above ordered compound [4]. It contains two additional O—H stretching modes and one additional lattice mode (see Table 1), but is otherwise identical. This shows that the basic structure is that of β-Ni(OH)$_2$, but with additional features which relate to an empirical formula with Ni/OH < 0.5. A structural model of a hydrated β-phase with interlamellar water can be written as shown in eqn. (3).

$$Ni(OH)_2 \cdot yH_2O \qquad\qquad\qquad (3)$$

The lack of molecular water vibrations in both the IR and Raman spectra suggest this hydrated model is inadequate. The lattice parameters observed for these disordered-β materials are comparable to those of ordered

β-Ni(OH)$_2$, and do not provide room for interlamellar H$_2$O molecules. Therefore this model is inadequate.

An alternative formulation with an equivalent stoichiometry, where $x = y/(2 + y)$, can be written (eqn. (4)).

$$Ni_{1-x}(2H)_x(OH)_2 \tag{4}$$

Nickel vacancy disorder is proposed based on the empirical nickel deficit ($x < 0.16$) and the vibrational spectra. A second type of disorder is possible. Layer stacking disorder is likely, based upon X-ray line broadening [9]. Recent EXAFS analyses support the nonstoichiometric model [10].

Charged active mass and discharged active mass

The chemically oxidized γ-NiOOH structure is the prototype for charged active mass [4]. This non-close packed NiOOH-type structure contrasts sharply with the close packed β-Ni(OH)$_2$ structure. The two lattice modes (Table 1), and the lack of an O–H stretching mode, originate from the non-close packed layer stacking (ABBCCA) and interlamellar hydrogens on centric lattice sites. This structure has been supported by re-interpretation of the X-ray diffraction pattern [4].

Both forms of charged active mass (3β- and 3γ-NiOOH) exhibit the same selection rules, which indicates that they have similar structures [3]. This crystal structure, together with the point defect structure, allows one to understand the origin of the variable formulae and oxidation states. The key difference between the 3β- and 3γ-NiOOH phases is the magnitude of the nickel deficit and the resultant point defect structures (see Table 2). The nickel deficit is constant within each cycle. The 3γ-phase generally contains potassium as well. The amount of potassium uptake is determined

TABLE 2

Comparison of empirical and nonstoichiometric formulae

Structural designation	Typical empirical formula				Ref.	Nonstoichiometric structural formula
	Ni	O	H	K		
Ordered β-Ni(OH)$_2$	1.00	2.00	2.00		[a]	β-Ni(OH)$_2$
Disordered β-Ni(OH)$_2$	1.00	2.35	2.70		[a]	Ni$_{0.85}$(2H)$_{0.15}$(OH)$_{2.0}$
Cathodic α-Ni(OH)$_2$	1.00	3.10	4.20		[a]	Ni$_{0.75}$(2H)$_{0.25}$OOH$_{2.0}$·0.33 H$_2$O
2α	1.00	2.67	3.09		15	Ni$_{0.75}$(H)$_{0.25}$OOH$_{2.1}$
3γ	1.00	2.68	1.36	0.33	16	Ni$_{0.75}$(K)$_{0.25}$OOH$_{1.0}$
2β	1.00	2.25	2.25		15	Ni$_{0.89}$V$_{0.11}$OOH$_{2.0}$
3β	1.00	2.24	1.55	0.03	16	Ni$_{0.89}$(3H)$_{0.08}$(K)$_{0.03}$OOH$_{1.14}$

[a]This work.

by the nickel deficit, *i.e.*, the nickel vacancies appear to be filled with potassium. The ramifications of this nonstoichiometric structure upon the electrochemical properties are significant [3]. The differing oxidation states allow the α/γ cycle to have a greater capacity. The nonstoichiometry and point defects also control proton diffusion and electron conduction.

Discharged active mass (2α- and 2β-phases) displays spectra and selection rules similar to those for charged active mass [4]. We propose a similar non-close packed layer structure. The nickel deficit in each is comparable with that in the respective charged phase (see Table 2).

The wavenumber positions vary with charge state and defect content (see Table 1) as the active mass is charged and discharged. The α/γ bands are higher in energy (wavenumber position) than the β/β bands. This shift parallels the increased nickel deficit observed for the α/γ phases. Therefore, the change in defect structure is also reflected in the band positions. The energy of a vibrational mode is proportional to the bond strength (*i.e.*, force constant). An increase in oxidation state normally leads to an increase in wavenumber [11]. The mechanism by which the nickel deficit influences wavenumber is the same, in that the change in nonstoichiometry induces an increase in average oxidation state and, thereby, an increase in wavenumber.

The traditional structures proposed for discharged active mass (2α and 2β) are β-Ni(OH)$_2$ or the so-called α-phase structure [2]. The Raman spectra of discharged active mass clearly demonstrate that formed and cycled materials are not isostructural with β-Ni(OH)$_2$ (compare spectra in Table 1) [3]. The Raman spectrum of a chemically precipitated α-phase also differs from that of discharged active mass (see Table 1). Therefore, the structures of chemical-α and 2α or 2β differ as well. The structural difference between discharged active mass (2α) and a cathodic-α phase precursor is more subtle and will be discussed below.

Implications of the nonstoichiometric structure of active mass

The oxidation state maximum seen for 3γ is +3.67. This oxidation state is predicted for a defect structure which incorporates potassium on 0.25 vacant nickel sites. With a +1 dopant (K) on the nominal Ni(III) site, only 2 electron holes remain per site to ionize and to form two Ni(IV) species. Ionization provides 0.5 moles of Ni(IV), eqn. (5), giving an average oxidation state of 3.67 for the total 0.75 moles of nickel per mole of compound.

$$Ni^{4+}_{0.5}Ni^{3+}_{0.25}(K^+)_{0.25}OOH \qquad (5)$$

Discharge of this material reduces the nickel, but the 0.25 protons on the nickel vacancies produce an average nickel oxidation state of 2.25 for the 2α-phase (see Table 2). It is apparent that the nickel cannot be reduced completely to 2.00 because the lattice requires charge balance and the vacant nickel site (nominally 2+ on the discharged lattice) holds only one proton (based upon the empirical formula).

The 3γ point defect structural model explains how Ni(IV) ions can be introduced into the nominally Ni(III), NiOOH-type crystal lattice. In order for the average oxidation state of nickel to exceed 3+, a nickel deficit is required. The 3β structure (Table 2) demonstrates that the nickel deficit is not the only prerequisite to an oxidation state above 3+. The dopant content, three protons on the nickel vacancy, reduces the average oxidation state to 2.9 in this case.

It has been observed that the nickel vacancies are invariably filled with protons or alkali metals, and that the excess monovalent cations fit exactly on the vacancies, within reasonable experimental error. When alkali metals are low, one to three protons can be found per vacancy. When sufficient alkali is present in the formula, it generally fills the vacancy. Therefore, when writing formulae, we have chosen to place potassium or sodium on the nickel vacancy sites in preference to interlamellar sites. We do this to demonstrate correlation of potassium content and vacancy content. This observation appears to suggest that the potassium on nickel site positioning is fact; however, it is important to realize that this may be coincidence. We have no positive, experimental evidence to prove this, nor to disprove it. It can be said that the potassium does stabilize the nickel deficit.

Thus the point defect structure (nickel deficit and dopant K or H contents) controls both the maximum oxidation state and the minimum oxidation state. Needless to say, the oxidation state change between the two extremes controls the electrode capacity. The same logic applies to the β/β cycle, with the result that the narrower oxidation state range leads to a lower capacity. Therefore, the nonstoichiometric model allows one to understand the variable oxidation states of nickel active mass as well as the variable capacities.

Cathodic-α precursors of active mass

The two Raman lattice modes observed for cathodically deposited electrode-precursor materials are consistent with a non-close packed structure. Although the cathodically deposited α-phase materials exhibit a broad O–H stretching mode, the lattice mode region differs little from that of discharged active mass (Table 1) [4]. Therefore the two structures are related in terms of layer stacking. X-ray powder diffraction data also reflect this similarity [1, 2]. However, the O–H stretching mode indicates that there are differences in water content and/or proton bonding. This structural difference may be significant.

The lattice mode positions (see Table 1) for the cathodic-α phase are lower than for the discharged active mass phases (2α and 2β). This shift is related to the difference in bond strengths associated with a small change in oxidation state. The cathodic-α material is green and is Ni(II). The oxidation states of the dark, discharged active mass are greater than 2 (see Table 3).

The empirical formula of a cathodic-α material is written in Table 2. The nickel–oxygen ratio in these materials is generally lower than for

TABLE 3

Solid state structural characteristics of active mass or active mass precursors based on spectral analysis

Structural designation	Ordered β-Ni(OH)₂	Disordered β-Ni(OH)₂	Cathodic α-Ni(OH)₂	Chemical α-Ni(OH)₂	Active mass			
					2α	3γ	2β	3β
Preparation method	Recrystallized	Rapid ppt., aged alpha	Electrochemical	Rapid ppt.	Electrochemical			
Layer–layer stacking	hcp	hcp	ncp	ncp	ncp	ncp	ncp	ncp
Ni average oxid. state*	2	2	2	2	2.25	3.67	2.25	2.90
Stoichiometry	stoi.	non.	non.	non.	non.	non.	non.	non.
Crystalline order	ord.	dis.	dis.	dis.	dis.	dis.	dis.	dis.
Molecular water content	no	slight	possible	possible	no	no	no	no

hcp = hexagonal close packed; ncp = non-close packed; stoi. = stoichiometric; non. = nonstoichiometric; ord. = ordered; dis. = disordered.

*Active mass oxidation states from ref. 15.

discharged active mass. This can be caused by either additional molecular water (eqn. (6)) or a more extensive nickel deficit (eqn. (7)).

$$Ni_{0.75}(2H)_{0.25}(OH)_2 \cdot 0.33\ H_2O \tag{6}$$

$$Ni_{0.65}(2H)_{0.35}(OH)_2 \tag{7}$$

We favor the molecular water explanation because the Raman spectrum of cathodic-α displays O–H stretching modes which are typical of water. The hypothetical nickel deficit in eqn. (7) is also greater than 0.25; the 0.35 value is larger than that seen in other materials to date.

The above results show that discharged active mass, charged active mass, and cathodic-α phases are non-close packed and related in structure. The proposal of this structure for the α-phases disagrees with literature, which suggests close packed inter-layer stacking [1]. The literature powder pattern has been assigned a low reliability in the JCPDS file [12] and has been questioned in the literature [13]. Further research is needed to understand how the excess "water" is incorporated structurally.

Cobalt-containing nickel electrodes: precursors and active mass

Raman spectra of cobalt-containing precursors, *i.e.*, cathodically deposited materials, are distinct, and differ from that of cobalt-free, cathodic-α phase [6]. The Raman spectrum of a 5% cobalt cathodic-α displays two Raman bands at 460 and 530 cm^{-1} (Fig. 1). The wavenumber positions are identical with those observed with no cobalt, but the intensity ratio for the two bands is inverted. A very weak O–H stretching mode is observed at 3652 cm^{-1}. The weakness of this band, and the intensity reversal, distinguish the cobalt-free and cobalt-containing spectra. These changes reflect the significant influence of cobalt addition. Changes in the electronic structure of the solid when the cobalt solid solution is formed apparently change the bonding enough to change the polarizability of these lattice modes. Raman intensities depend directly upon the polarizability tenser associated with each normal vibration.

However, the spectral selection rules do not change with cobalt addition for these cathodically deposited materials. The spectra are therefore consistent with a non-close packed structure, with the cobalt going into solid solution on the nickel sites. We propose the layer stacking is ABBCCA, similar to active mass without cobalt.

Formation and cycling of the above materials produce an active mass material that displays Raman spectra similar to those of cobalt-free, nickel electrode active mass [3]. The fact that the active mass spectral selection rules do not change upon cobalt addition indicates that the cobalt is incorporated in solid solution, and that a non-close packed structure is retained. The previous discussion of active mass structure applies to cobalt-containing active mass as well.

Cobalt addition introduces a structure that is intermediate between the β/β and α/γ stoichiometries. Both the Raman spectral positions (550
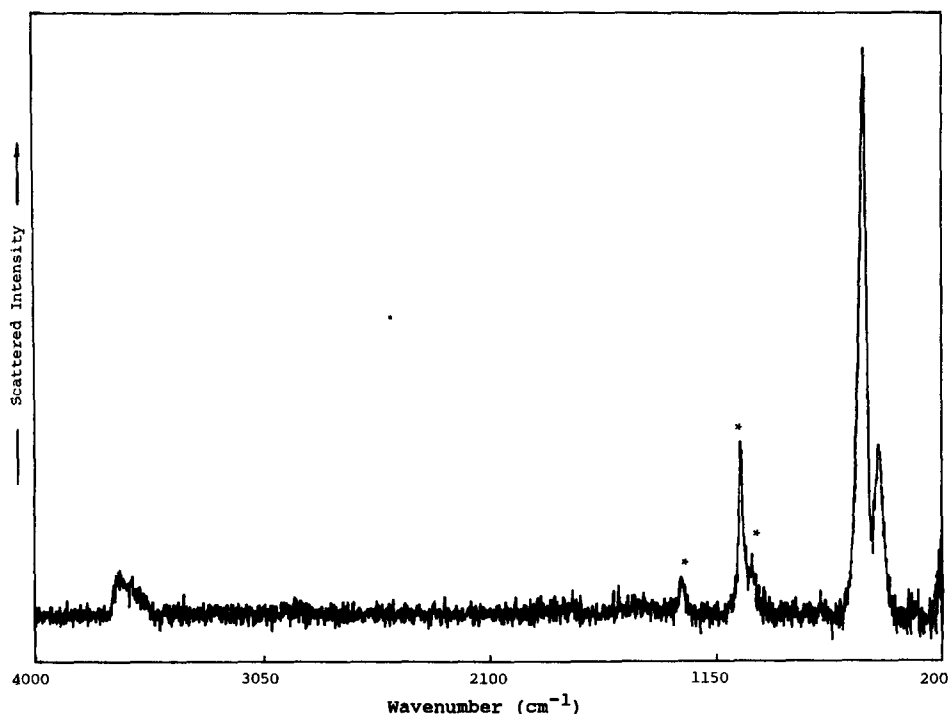
Fig. 1. Raman spectrum of cathodic-α nickel electrode with 5% cobalt additive. Bands marked with an asterisk are nitrate vibrational modes.

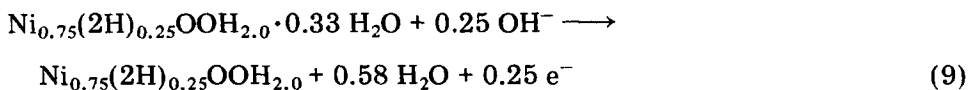and 474 cm^{-1}, charged) and empirical formulae suggest this [3]. The recent cobalt-containing empirical formula reported by Braconnier *et al.* can be recast in nonstoichiometric form in eqn. (8) [14]. The nickel deficit obtained is 0.19, falling between the cobalt-free β/β and α/γ values, as expected (based upon Raman spectral positions). It is apparent that the cobalt stabilizes an increased cation deficit.

$$Ni_{0.57}Co_{0.24}K_{0.17}Na_{0.02}OOH_{0.92}Na_{0.08} \tag{8}$$

Structural and chemical changes

The formation process

Both cathodic-α and active mass are nonstoichiometric and non-close packed. Therefore, no change in layer stacking is required during the formation process. If the cathodic-α precursor contains a significant nickel deficit, then the change in nickel nonstoichiometry during formation can be minimal. For example, a cathodic-α (eqn. (6)) would form an active mass, as defined in eqn. (9), if no change in nickel deficit occurred. A net loss in "water" is evident as well as a change in oxidation state.

$$Ni_{0.75}(2H)_{0.25}OOH_{2.0} \cdot 0.33\ H_2O + 0.25\ OH^- \longrightarrow$$

$$Ni_{0.75}(2H)_{0.25}OOH_{2.0} + 0.58\ H_2O + 0.25\ e^- \tag{9}$$

The formation of active mass from a more stoichiometric precursor would also involve creation of nickel vacancies. The final nickel deficit characterizing an active mass need not be equal to, nor controlled by, the deficit in the precursor-α. The formation process can increase the nickel deficit to form more optimal active mass.

Transformation of a cathodic-α to active mass involves a change in proton incorporation or bonding, as demonstrated by the loss of the O–H stretching mode upon formation. This change in the spectrum is consistent with our proposal that the cathodic-α contains molecular water which is removed or lost during formation.

A stoichiometric precursor with close packed stacking, such as β-$Ni(OH)_2$, must undergo major structural change upon formation into non-stoichiometric, non-close packed active mass. Both transformation from close packed to non-close packed layer stacking and vacancy creation are required. It is likely that layer shearing and defect formation processes would slow the formation process for such starting materials. Furthermore, shape and volume changes are expected to be much greater for such a precursor. It is likely that these would reduce the electrode mechanical integrity as well. We propose that the reason that cathodically deposited materials are successful precursors to active mass is intimately tied to the minimal structural change required during the formation process.

Charge and discharge cycling and transformation from β/β to α/γ cycles

Shifts in band position during charging and discharging of cobalt-free active mass directly reflect changes in the structure and bonding which occur as the nickel oxidation state varies (Table 1). The wavenumbers increase during charging and drop on discharge, as discussed earlier. The general charge–discharge reaction can be written as shown in eqn. (10). K^+ may replace x of the protons to give the α/γ cycle. If no overcharging occurs the structural changes are simply changes in proton content and oxidation state. No change in defect structure or layer stacking is required.

$$Ni_{1-x}(nH)_xOOH_2 + [1 + x(n-1)]OH^- \longrightarrow$$

$$Ni_{1-x}H_xOOH_{1.0} + [1 + x(n-1)]H_2O + [1 + x(n-1)]\ e^- \tag{10}$$
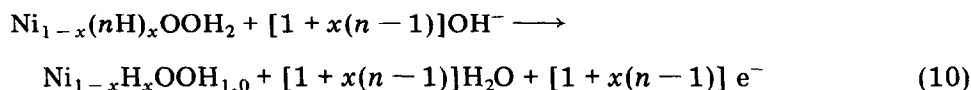
Overcharging a 3β-material induces the 3γ-phase [2]. As seen in the nonstoichiometric formulae (Table 2) the materials in the two cycles display different nickel deficits. We propose that overcharging induces the higher level of nonstoichiometry to accommodate the higher oxidation state formed during overcharge. The resultant point defect structure allows a greater change in oxidation state, which provides the higher capacity observed for the α/γ cycle. A significant amount of potassium is introduced

when 3γ is produced. It is apparent that the potassium and the increased nickel deficit are important to the stability of this structure.

Once formed, retention of the α/γ cycle might be expected. However, further cycling will allow transformation back to the β/β cycle with a concomitant reduction in nickel deficit and potassium content. Furthermore, these are not the only structural changes expected with this model. One mechanism for return to the β/β cycle involves ageing of discharged-α to disordered β-Ni(OH)$_2$ (as described below), with subsequent cycling and re-formation back into the β/β cycle. The intermediate structure is close packed (disordered β-Ni(OH)$_2$). Because this mechanism involves a change in layer–layer stacking, density and volume changes are expected. Therefore, both mechanical stability and capacity would be reduced. This is consistent with experimental observations.

Ageing in KOH

The product of KOH ageing of a cathodic-α was found to be "de-activated-α" by Barnard *et al.* [15]. The Raman spectrum of such an aged material shows that it is a nonstoichiometric, disordered-β compound [4]. Barnard *et al.* observed a β-like X-ray pattern as well, but did not differentiate it as a nonstoichiometric material [9].

The role of cobalt addition

The mechanisms by which cobalt has a beneficial effect on electrode properties can now be discussed in terms of the structures and structural changes already defined. Cobalt is incorporated in solid solution with nickel in cathodic-α and active mass. All three materials are non-close packed. Cobalt stabilizes nickel deficit nonstoichiometry that is higher than for cobalt-free systems. This structure enhances electrochemical properties, including a higher nickel oxidation state.

Another role of the cobalt additive appears to be in stabilizing a cathodically-deposited precursor structure, with enhanced nonstoichiometry, which is structurally similar to optimal active mass. The very weak O–H stretching mode observed with cobalt addition is a measure of a water, proton, and defect content more like that of active mass. This will improve mechanical stability by minimizing the density and volume changes during formation. The optimal nonstoichiometry and point defect structure will also optimize the electronic and protonic diffusion processes.

Conclusions

Optimal nickel active mass is non-close packed and nonstoichiometric, as is cathodic-α. The formation process transforms precursor phases into this structure. Therefore, the precursor nonstoichiometry and disorder, or lack thereof, influence the final active mass structure and the rate of formation. Ageing to less active material, or incorporation of less than

optimum nonstoichiometry, reduces capacity. The role of cobalt addition can be appreciated in terms of structures favored or stabilized by the dopant.

The unique spectral signatures found for the various phases allow differentiation of these materials and reflect significant structural variations. Most importantly, the layer stacking is clearly indicated by Raman spectroscopic analysis. The nonstoichiometry allows one to understand the oxidation states and electrochemical properties. An optimum active mass will exhibit an enhanced nickel deficit, providing a maximum change in oxidation state, and will resist ageing. How formation of such a material can increase mechanical stability is discussed in terms of a structurally similar precursor-α.

This new structural understanding provides a basis upon which one can study the subtle structural effects induced by empirical parameters such as cobalt concentration or electrolyte concentration. With such information the electrode structure can be tuned to provide optimal electrochemical properties. It should be possible to relate optimal structure of a precursor-α, and of formed active mass, to properties during cycling. Furthermore, the potential of Raman spectroscopy for quality control purposes appears bright because the spectra vary qualitatively to mirror both major and subtle variations.

Acknowledgement

References

1 H. Bode, K. Dehmelt and J. Witte, *Electrochim. Acta, 11* (1966) 1079 - 1087.
2 H. Bode, K. Dehmelt and J. Witte, *Z. Anorg. Allg. Chem., 366* (1969) 1 - 21.
3 P. L. Loyselle, P. J. Karjala and B. C. Cornilsen, A point defect model for nickel electrode structures, in J. R. Selman and H. C. Maru (eds.), *Proc. Symp. on Electrochemical and Thermal Modeling of Battery, Fuel Cell, and Photoenergy Conversion Systems,* Electrochemical Society, Pennington, NJ, 1986, pp. 114 - 121.
4 B. C. Cornilsen, P. J. Karjala and P. L. Loyselle, *J. Power Sources, 22* (1988) 351 - 357.
5 P. Oliva, J. Leonardi, J. F. Laurent, C. Delmas, J. Braconnier, M. Figlarz, F. Fievet and A. deGuibert, *J. Power Sources, 8* (1982) 229 - 255.
6 X. Shan, P. L. Loyselle and B. C. Cornilsen, Structural influence of cobalt addition to the nickel electrode, *174th Electrochem. Soc. Meeting, Chicago, IL, October 14, 1988,* Abstr. 79.
7 P. M. De Wolff, Joint Committee on Powder Diffraction Standards, Card No. 14-117.
8 A. Szytula, A. Murasik and M. Balanda, *Phys. Status Solidi B, 43* (1971) 125 - 128.
9 R. Barnard, C. F. Randell and F. L. Tye, Studies concerning the ageing of alpha and beta Ni(OH)$_2$ in relation to nickel–cadmium cells, in J. Thompson (ed.), *Power Sources 8,* Academic Press, London, 1981, pp. 401 - 423.

10 P. L. Loyselle, B. C. Cornilsen, R. A. Condrate and J. C. Phillips, X-ray absorption study of beta nickel hydroxides, *174th Electrochem. Soc. Meeting, Chicago, IL, October 14, 1988*, Abstr. 77.

11 K. Nakamoto, *Infrared and Raman Spectra of Inorganic and Coordination Compounds*, Wiley, New York, 1986.

12 H. Bode, Joint Committee on Powder Diffraction Standards, Card No. 22-444.

13 R. S. McEwen, *J. Phys. Chem.*, *75* (1971) 1782 - 1789.

14 C. Delmas, J. J. Braconnier, Y. Borthomieu and P. Hagenmuller, *Mater. Res. Bull.*, *22* (1987) 741 - 751.

15 R. Barnard, C. F. Randell and F. L. Tye, *J. Appl. Electrochem.*, *10* (1980) 109 - 125.

16 R. Barnard and C. F. Randell, *J. Appl. Electrochem.*, *12* (1982) 27 - 38.